$CD4^+$ T-cell–independent mechanisms suppress reactivation of latent tuberculosis in a macaque model of HIV coinfection

Taylor W. Foreman[a,b,1], Smriti Mehra[a,c,d,1], Denae N. LoBato[a], Adel Malek[e], Xavier Alvarez[a], Nadia A. Golden[a], Allison N. Bucşan[a,b], Peter J. Didier[a], Lara A. Doyle-Meyers[a], Kasi E. Russell-Lodrigue[a], Chad J. Roy[a], James Blanchard[a], Marcelo J. Kuroda[a], Andrew A. Lackner[a,b], John Chan[e], Shabaana A. Khader[f], William R. Jacobs Jr.[e,g,2], and Deepak Kaushal[a,b,2]

[a]Tulane National Primate Research Center, Covington, LA 70471; [b]Department of Microbiology and Immunology, Tulane University School of Medicine, New Orleans, LA 70112; [c]Center for Biomedical Research Excellence, Louisiana State University School of Veterinary Medicine, Baton Rouge, LA 70803; [d]Department of Pathobiological Sciences, Louisiana State University School of Veterinary Medicine, Baton Rouge, LA 70803; [e]Department of Microbiology and Immunology, Albert Einstein College of Medicine, Bronx, NY 10461; [f]Department of Molecular Microbiology, Washington University School of Medicine, St. Louis, MO 63110; and [g]Howard Hughes Medical Institute, Albert Einstein College of Medicine, Bronx, NY 10461

Contributed by William R. Jacobs Jr., July 27, 2016 (sent for review June 10, 2016; reviewed by Ashley T. Haase and Frank A. W. Verreck)

The synergy between *Mycobacterium tuberculosis* (*Mtb*) and HIV in coinfected patients has profoundly impacted global mortality because of tuberculosis (TB) and AIDS. HIV significantly increases rates of reactivation of latent TB infection (LTBI) to active disease, with the decline in $CD4^+$ T cells believed to be the major causality. In this study, nonhuman primates were coinfected with *Mtb* and simian immunodeficiency virus (SIV), recapitulating human coinfection. A majority of animals exhibited rapid reactivation of *Mtb* replication, progressing to disseminated TB and increased SIV-associated pathology. Although a severe loss of pulmonary $CD4^+$ T cells was observed in all coinfected macaques, a subpopulation of the animals was still able to prevent reactivation and maintain LTBI. Investigation of pulmonary immune responses and pathology in this cohort demonstrated that increased $CD8^+$ memory T-cell proliferation, higher granzyme B production, and expanded B-cell follicles correlated with protection from reactivation. Our findings reveal mechanisms that control SIV- and TB-associated pathology. These CD4-independent protective immune responses warrant further studies in HIV coinfected humans able to control their TB infection. Moreover, these findings will provide insight into natural immunity to *Mtb* and will guide development of novel vaccine strategies and immunotherapies.

Nonhuman primate | B cells | tuberculosis | CD4 T cells | CD8 T cells

The emergence of AIDS in the 1980s resulted in the syndemic relationship with tuberculosis (TB), whereby progression of each infection exacerbates the other disease (1). Early studies in the murine model highlighted the role for $CD4^+$ T cells in the control of *Mycobacterium tuberculosis* (*Mtb*) (2), and the initial observations that HIV-induced $CD4^+$ T-cell depletion correlated with increased risk of TB disease cemented this paradigm (3, 4). $CD4^+$ T cells respond to infected pulmonary macrophages and limit bacterial growth through synergistic IFN-γ/TNF-α signaling (5); these responses to foci of infected macrophages initiate the formation of the tuberculoid granuloma, which is composed of lymphocytes, macrophages, dendritic cells, and neutrophils (6). The granuloma acts to contain bacteria; however, the events that ensue upon interaction of *Mtb* with the host can result in microenvironmental changes, leading to an enduring subclinical infection defined as latent TB infection (LTBI) (7, 8). Despite the critical role of $CD4^+$ T cells, their influx into granulomas does not necessarily correlate with protection (9). Furthermore, some coinfected patients retain increased risk of reactivation despite maintaining $CD4^+$ T-cell counts, and the complete causality of reactivation remains unknown. Nonetheless, $CD4^+$ T-cell depletion because of HIV infection remains the prominent justification for increased rates of LTBI reactivation.

Although the innate immune response to TB infection initializes protective responses (10), the granuloma is neither structurally nor functionally complete without T cells that recognize specific *Mtb* antigens (11). $CD8^+$ T cells have an essential but underappreciated role in the control of TB (12) and are critical for both natural and vaccine-induced immunity in nonhuman primates (NHPs) (13, 14). In contrast, the role of B cells in immunity to TB is less well understood, although it appears they are required for the development of optimal immune responses to *Mtb* via various regulatory mechanisms (15–17).

HIV dysregulates many aspects of TB immunity by causing chronic immune activation (18), skewing the T_{reg}/T_H17 balance (19), and perturbing B-cell signaling and memory formation (20). HIV further blocks TNF-α–mediated macrophage activation and apoptosis, thus favoring the persistence of *Mtb* (21). Whereas these studies have been informative, the detailed immunological regulation of LTBI reactivation as a result of HIV coinfection remains to be completely defined.

Significance

According to the World Health Organization, one in three humans is latently infected with *Mycobacterium tuberculosis* and 10% of these individuals risk developing active, clinical tuberculosis (TB) over their lifetimes. Coinfection with human immunodeficiency virus increases this risk substantially, with depletion of $CD4^+$ T cells believed to drive disease progression. Although a minority of coinfected individuals can control the infection, the mechanisms underlying this phenomenon remain unknown. Modeling coinfection using macaques, we discovered that one-third of the animals maintained latency despite complete ablation of lung $CD4^+$ T cells. We report that protective immune responses mediated by $CD8^+$ T cells and B cells correlate with TB control. These findings have important implications in development of both prophylactic and therapeutic measures against TB and acquired immunodeficiency syndrome.

Author contributions: D.K. designed research; T.W.F., S.M., X.A., N.A.G., A.N.B., P.J.D., A.A.L., and D.K. performed research; L.A.D.-M., K.E.R.-L., C.J.R., J.B., S.A.K., and D.K. contributed new reagents/analytic tools; T.W.F., S.M., D.N.L., A.M., X.A., M.J.K., J.C., S.A.K., W.R.J., and D.K. analyzed data; and T.W.F., A.M., A.A.L., J.C., W.R.J., and D.K. wrote the paper.

Reviewers: A.T.H., University of Minnesota; and F.A.W.V., Biomedical Primate Research Centre.

The authors declare no conflict of interest.

[1]T.W.F. and S.M. contributed equally to this work.

[2]To whom correspondence may be addressed. Email: jacobsw@hhmi.org or dkaushal@tulane.edu.

This article contains supporting information online at www.pnas.org/lookup/suppl/doi:10.1073/pnas.1611987113/-/DCSupplemental.

Macaques serve as excellent models of human *Mtb*/HIV coinfection because they can establish LTBI and are susceptible to simian immunodeficiency virus (SIV), providing a valuable surrogate model for pathogenic HIV infection (22–26). Coinfected macaques recapitulate key aspects of the human disease, including $CD4^+$ T-cell depletion, reactivation of LTBI, and dissemination of the bacilli (22, 25). As part of the current investigation, we sought to understand the dynamics of TB disease progression following high-dose SIV coinfection in rhesus macaques and to establish the correlates associated with reactivation of LTBI. Our results indicate that a significant minority of macaques with LTBI did not exhibit reactivation immediately after SIV coinfection, despite productive viremia and substantial depletion of pulmonary $CD4^+$ T cells during the acute phase of SIV infection. Instead, protective immune responses were characterized by memory $CD8^+$ T-cell proliferation and the expanded presence of bronchus-associated lymphoid tissue (BALT), correlating with increased control of LTBI after SIV coinfection.

Results

Clinical Correlates of Infection During *Mtb*/SIV Coinfection. Thirty-seven macaques were exposed to low-dose aerosols of *Mtb* CDC1551, delivering ∼25 colony-forming units (CFUs) into the lungs (Fig. 1*A*). Delivery in a low dose, as opposed to a high dose (e.g., 1,000 CFUs) (14) or intermediate dose (e.g., 100 CFUs) (26), was used to establish a state of LTBI devoid of clinical signs of active TB. All animals were infected by *Mtb*, as evidenced by conversion of tuberculin skin test (TST) and PRIMAGAM (Table S1). Macaques remaining TST/PRIMAGAM-positive at 7 wk postinfection but not exhibiting symptoms of disease, such as elevated serum C-reactive protein (CRP), high thoracic radiograph (chest X-rays, CXR) scores, or the presence of culturable *Mtb* in bronchoalveolar lavage (BAL), were deemed asymptomatic and the infection was classified as latent TB (LTB). The quantifiable measures described above were paired with inputs from our veterinarians about respiratory rates, anorexia, pyrexia, and progressive weight loss.

Of the 37 animals exposed to *Mtb*, 10 animals developed active TB (ATB) and were excluded from the subsequent LTB/reactivation protocol. This subset and six historical controls ($n = 16$) were used to obtain clinical, microbiological, and lung pathology data for comparison and were defined as the ATB control group (Fig. 1 *A* and *B*). Twenty-seven animals did not show signs of ATB by week 9 after *Mtb* infection, such as progressive weight loss (Fig. 1*C*), pyrexia (Fig. 1*D*), CRP elevation (Fig. 1*E*), or radiological presence of pulmonary granulomatous disease (Fig. 1*F*). This group was classified as the LTB group and animals were randomly divided into two subgroups either to receive SIV intravenously (defined

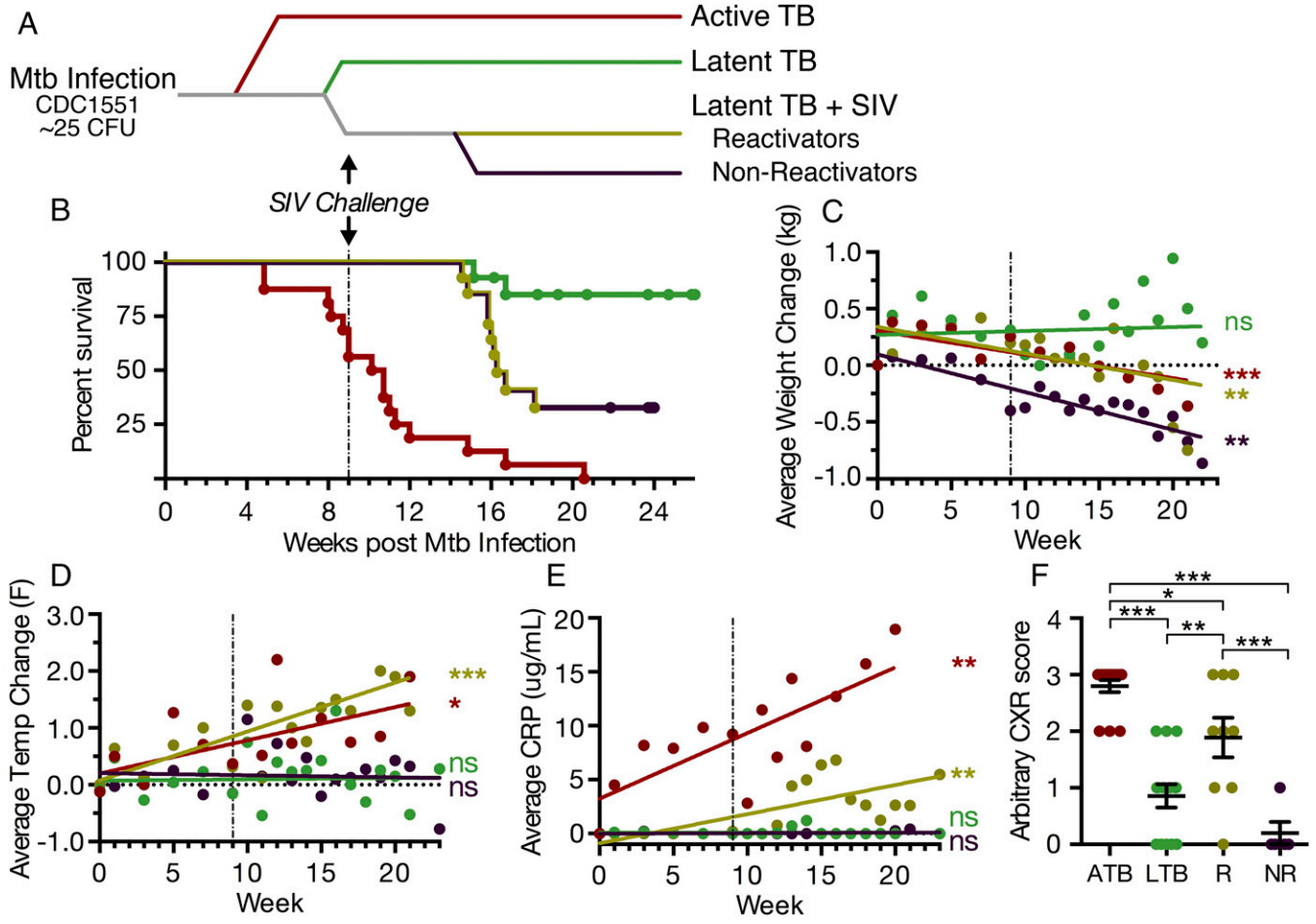

Fig. 1. Clinical correlates of *Mtb*/SIV coinfection. (*A*) Schematic indicating the different animal groups under study and marking key time points shown in *B*. Thirty-seven Indian rhesus macaques were infected with a low dose of *Mtb* CDC1551 (∼25 CFU). Coinfected animals were injected with $SIVmac_{239}$, and LTB control animals were injected with saline only. (*B*) Survival curves, displayed as days after *Mtb* infection. Dashed vertical line indicates day of SIV infection. (*C*) Linear regressions over time of average weight change (in kilograms); (*D*) average temperature change (in °F); (*E*) average serum CRP values (μg/mL); and (*F*) CXR scores, in the four groups: ATB, active TB (red); LTB, latent TB (green); R, coinfected reactivators (gold); NR, coinfected nonreactivators (purple). $*P < 0.05$, $**P < 0.01$, $***P < 0.001$ using (*B*) Wilcoxon test, (*C*–*E*) Linear regression analysis, and (*F*) one-way ANOVA. Data are means ± SD.

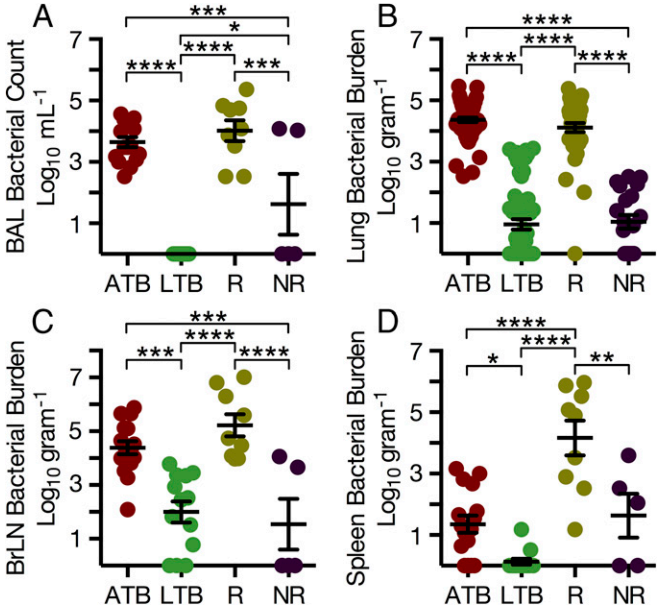

Fig. 2. Bacterial burden in lungs and extrathoracic organs. (*A*) *Mtb* CFUs in total BAL samples and (*B*) per gram of lung tissue at killing shown for each animal, with multiple sections of lung sampled per animal; active TB (ATB), latent TB (LTB), reactivator (R) and nonreactivator (NR) groups. (*C* and *D*) Bacterial burdens per gram of tissue for (*C*) bronchial lymph node and (*D*) spleen. *$P < 0.05$, **$P < 0.01$, ***$P < 0.001$, ****$P < 0.0001$, one-way ANOVA with Tukey's multiple testing correction.

as the LTB test group, $n = 14$), or remain SIV-naive (defined as the LTB control group, $n = 13$).

Survival was used as a key reporter of reactivation. Animals developing extensive TB after SIV coinfection were termed reactivators, and these animals were humanely killed at prescribed time points after evaluation by our veterinarian, as described in detail in *Materials and Methods*. Nine *Mtb*/SIV coinfected animals of 14 (~64%) in the LTB test group showed reactivated TB and were killed within 13–19 wk after *Mtb* infection. Five coinfected animals (~36%) survived, did not meet the clinical criteria for reactivated TB, and were termed nonreactivators (Fig. 1 *A* and *B*). This cohort was killed 19–21 wk after *Mtb* infection for collection of tissues for analysis following necropsy. Although these animals maintained LTBI throughout acute SIV infection, they did not develop AIDS within the 10–12 wk after SIV challenge. A majority of the animals in the LTB control group (11 of 13, 84%) and none of the animals in the active control group (0 of 16, 0%) survived to the termination of the study (Fig. 1*B*). Two animals in the LTB control group spontaneously reactivated despite remaining SIV-uninfected throughout the study. The survival difference between the coinfected animals in the LTB test group and the animals in the LTB control group was significant, using both a Wilcoxon ($P = 0.0002$) and a log-rank ($P = 0.0005$) test.

As expected, the ATB control group displayed significant weight loss, recapitulating the wasting seen in human TB (Fig. 1*C*). Subsequent to SIV coinfection, both reactivators and nonreactivators exhibited significant weight loss compared with the LTB control group, likely because of progressive SIV infection (Fig. 1*C*). Unlike with weight loss, for pyrexia, results for reactivators were significantly different from those of both nonreactivators and the LTB control group, with temperature increases similar to those of the ATB control group (Fig. 1*D*). The reactivators and ATB group also displayed higher CRP levels in the peripheral blood, an indication of severe inflammation (Fig. 1*E*), and they exhibited identical patterns when CXRs were analyzed for the severity of granulomatous disease (Fig. 1*F*). Together, these clinical manifestations highlight the robustness of the NHP model of coinfection for emulating human active, latent, and reactivated TB.

Microbiological Aspects of ATB, LTB, and Coinfection. We investigated the bacterial burden in BAL and various organs of the infected macaques following euthanasia. Following SIV infection, reactivators exhibited mean BAL CFU values significantly higher (10^4) than those of nonreactivators (~10^2) or animals in the LTB control group, with results indistinguishable from those of animals with ATB (Fig. 2*A*). Interestingly, two of five nonreactivating animals showed detectable, culturable *Mtb* in BAL at the endpoint of the study, indicating potential late reactivation (Fig. 2*A*). An approximate mean of 100 bacilli per gram could be cultured from the lung of animals with LTB, indistinguishable from the nonreactivators ($P = 0.988$), whereas a highly significant, ~100-fold increase in bacilli could be cultured from the lungs of reactivators (Fig. 2*B*); these reactivators had as much culturable *Mtb* in their lungs as animals with ATB (10^4 CFU per gram). We also measured *Mtb* burdens in extrathoracic tissues,

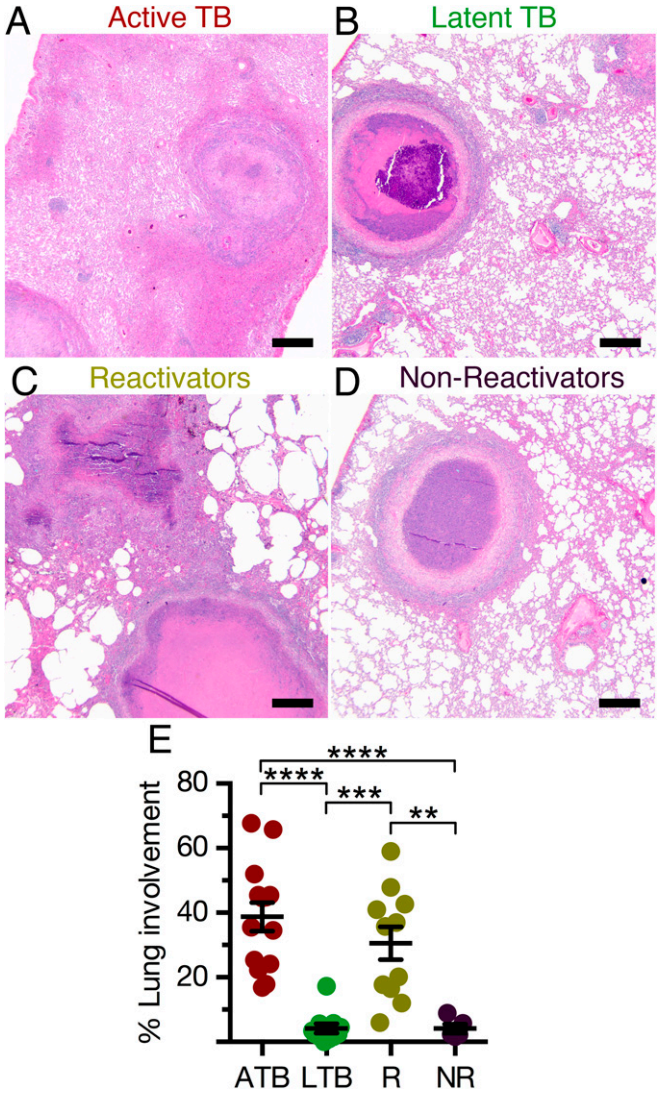

Fig. 3. Comparative TB pathology. H&E staining of lung sections from animals with (*A*) ATB, (*B*) LTB, (*C*) *Mtb*/SIV coinfected reactivators, and (*D*) *Mtb*/SIV coinfected nonreactivators. (*E*) Quantification of overall pathology as percentage of lung involvement. (Scale bars, *A–D*, 250 μ.) **$P < 0.01$, ***$P < 0.001$, ****$P < 0.0001$, using a one-way ANOVA with Tukey's multiple testing correction.

including bronchial lymph node (Fig. 2*C*), spleen (Fig. 2*D*), liver (Fig. S1), and kidney (Fig. S1). In bronchial lymph node, the CFU burden in both the ATB group and reactivators was significantly higher than in the LTB control group and nonreactivators (Fig. 2*C*). In general, reactivators not only harbored greater bacterial burden in their spleen, liver, and kidney relative to LTB and nonreactivators but also relative to animals with ATB. These microbiological results display similar qualities to human TB/HIV coinfection, where high bacterial burden and increased dissemination have been well documented (27, 28).

Peripheral Viral Loads. Because differential viral replication and titers could possibly explain the differences in the reactivator versus nonreactivator subgroups with respect to reactivation, we measured plasma viral loads after SIV infection in four randomly selected animals from both groups, using previously described methods (22) (Fig. S1). The mean $\log_{10}$ plasma viral load at 2 wk after SIV was 7.02 and 6.70 for reactivators and nonreactivators, respectively, and these differences were not significant. Plasma viral loads were not significantly different between the two groups at any time point, clearly suggesting that disparate peripheral viral loads were not the reason for differential reactivation of LTB in the two subsets of the LTB test group.

TB- and SIV-Associated Pathology. The pulmonary pathology analyses correlated well with clinical and microbiological findings. Coinfected animals that reactivated exhibited significantly more pulmonary lesions relative to nonreactivators and animals from the LTB control group, as determined by gross (Fig. S2) and histopathological examination (Fig. 3 *A*–*D*), and by morphometric quantitation (Fig. 3*E*). Thus, the LTB control group animals (Fig. 3*B*) and nonreactivators (Fig. 3*D*) had significantly fewer granulomas, with an average of 4–5% of the total lung area affected by TB lesions. These animals also displayed reduced TB-related

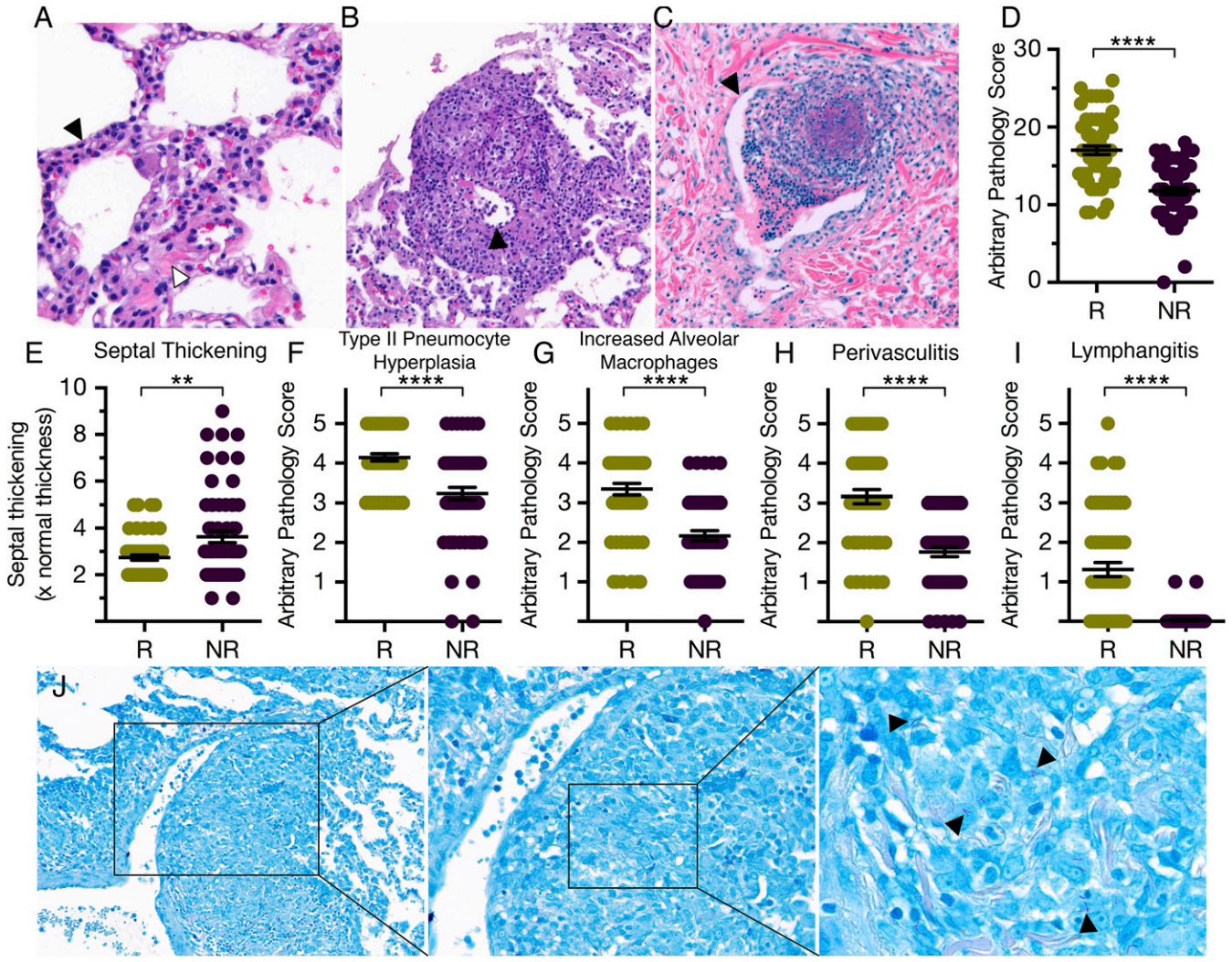

Fig. 4. SIV-induced pathology and the presence of bacilli perivascular lesions. H&E staining of lung sections from *Mtb*/SIV coinfected reactivators and nonreactivators displayed exacerbated pathology, including (*A*) interstitial pneumonia with septal thickening (white arrowhead), type II pneumocyte hyperplasia (black arrowhead), and lymphohistiocytic infiltration; (*B*) perivasculitis (black arrowhead showing blood vessel wall); and (*C*) lymphangitis (black arrowhead showing lymphatic vessel membrane). (*D*–*I*) Multiple lung sections from reactivators and nonreactivators were scored in a single-blinded fashion by a board-certified veterinary pathologist and quantitatively compared as (*D*) total SIV-induced pathology, (*E*) septal thickening, (*F*) type II pneumocyte hyperplasia, (*G*) increased alveolar macrophages, (*H*) perivasculitis, and (*I*) lymphangitis. Samples from three animals in each group were analyzed, with 12 lung sections analyzed per animal. Each dot corresponds to a section analyzed. $^{**}P < 0.01$; $^{****}P < 0.0001$ using Student's *t* test. (*J*) Ziehl–Neelsen staining revealed the presence of numerous intact, rod-like tubercle bacilli, indicated by black arrowheads in a perivascular lesion in a reactivator. *Right* panel is a magnified image of the boxed region from *Left* and *Center* panels. (Magnification, *A*, 50×; *B*, *C*, and *J*, 40×.)

pathology, inclusive of edema, pneumonia, and generalized foci of inflammation. In contrast, reactivators (Fig. 3*C*) displayed ∼30% lung involvement on average, comparable to an average involvement of ∼40% of the lung of animals with ATB (Fig. 3*E*). Importantly, the differences in the extent of lung pathology between reactivators and nonreactivators were highly significant ($P = 0.004$), despite a smaller group size for the latter (Fig. 3*E*).

All coinfected animals demonstrated lesions consistent with SIV-induced pulmonary pathology, including lymphohistiocytic interstitial pneumonia and septal thickening (Fig. 4 *A* and *E*), type II pneumocyte hyperplasia (Fig. 4 *A* and *F*), increased accumulation of foamy alveolar macrophages (Fig. 4*G*), lymphocytic perivasculitis (Fig. 4 *B* and *H*), and lymphangitis (Fig. 4 *C* and *I*). Whereas all coinfected animals displayed signs of SIV-induced pathology, reactivators showed significantly increased total pathology (Fig. 4*D*). Moreover, reactivators scored higher than nonreactivators on each measure of pathology (Fig. 4 *F*–*I*), with the exception of septal thickening (Fig. 4*E*). Finally, Ziehl–Neelsen staining revealed a high bacterial burden in the lymphocytic perivasculitis lesions, suggesting a possible causality of dissemination to extrathoracic organs (Fig. 4*J*).

Although the peripheral viral loads were comparable, the increased SIV-associated pathology may suggest increased viral replication in the lung of reactivators. We therefore further assessed pulmonary viral replication by analyzing lung sections for the presence of SIV mRNA by in situ hybridization. Viral titers in serum were similar among all SIV coinfected animals, whereas reactivators harbored significantly more SIV-infected cells (Fig. 5). Although the majority of cells infected by SIV were $CD3^+$ T cells (Fig. 5*C*), a few macrophages ($CD68^+CD163^+$) were also SIV^+ (29). These data, together with the increased TB-associated pathology, demonstrate that both pathogens appear to synergize to overcome the immune control at the microenvironmental level of the granuloma.

Immune Correlates of *Mtb*/SIV Coinfection. We studied the accumulation of various immune cell types in both whole blood and BAL in a subset of animals from each coinfected group to investigate the kinetics and mechanisms of SIV-mediated reactivation of LTBI in macaques. SIV coinfection led to a massive depletion of $CD4^+$ T cells in the lungs of all coinfected animals. The percentages of $CD4^+$ T cells in BAL of reactivators and nonreactivators dropped to 2.6% and 2.8%, respectively, of $CD3^+$ T cells 3 wk after SIV infection (Fig. 6*A*), in contrast to ∼31% in the LTB control group. Notably, the depletion of $CD4^+$ T cells in peripheral blood was actually significantly greater in nonreactivators, comprising 26% of $CD3^+$ lymphocytes compared with 40% in reactivators (Fig. 6*B*). Greater depletion of $CD4^+$ T cells in tissues relative to the peripheral blood following SIV infection is well documented in both humans and macaques (30), and this was consistent with our findings that the fold-change in the CD4:CD8 ratio in the BAL of reactivators and nonreactivators was ∼12- and 13-fold, respectively (Fig. 6*C*). In contrast, the comparative change in whole blood was only ∼twofold in both reactivators and nonreactivators (Fig. 6*C*). These findings demonstrate the comparable extent of $CD4^+$ T-cell depletion from the lungs of animals with two distinct clinical outcomes after SIV coinfection. Moreover, the absolute numbers of $CD4^+$ T cells in BAL of reactivators and nonreactivators were not significantly different (Fig. S3). Consistent with our findings in BAL, $CD4^+$ T cells taken from the lung at killing displayed similar frequencies, comprising ∼4% of total $CD3^+$ T cells (Fig. S3). Furthermore, characterization of lung sections by staining showed comparable spatial distributions of $CD4^+$ cells in pulmonary lesions from both reactivators and nonreactivators (Fig. S3). Taken together, these data demonstrate that comparable depletion of $CD4^+$ T cells occurred in both reactivators and nonreactivators and therefore that this depletion is not responsible for the varying clinical outcomes among the coinfected macaques.

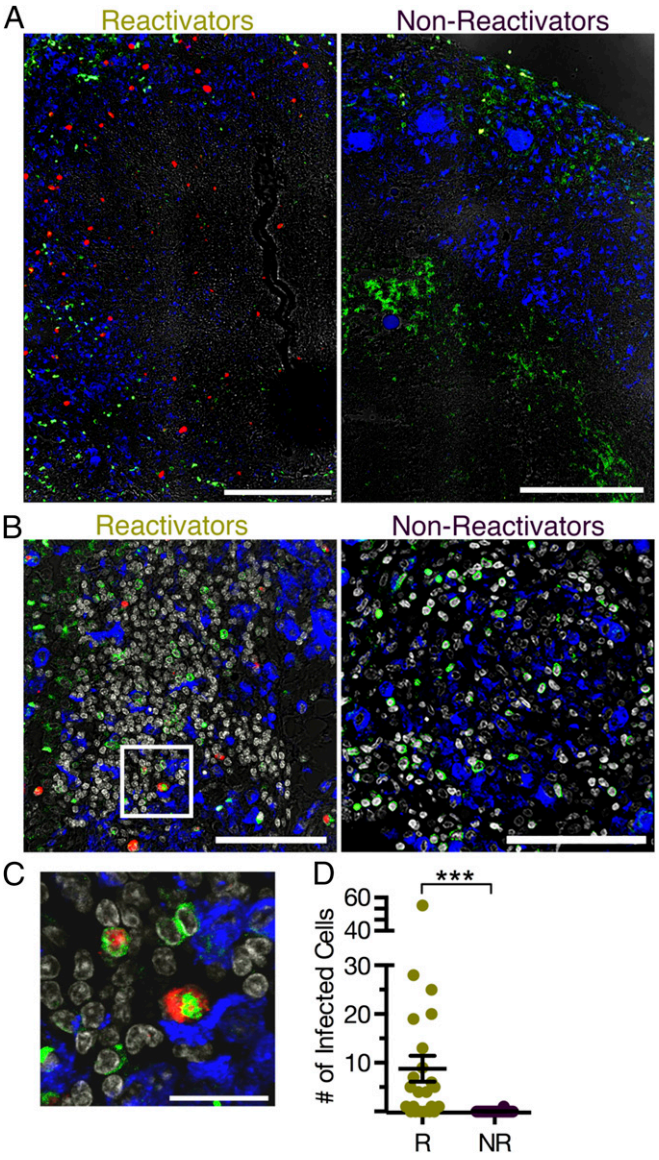

Fig. 5. SIV-infected cells in the granulomas of coinfected animals. (*A* and *B*) In situ hybridization of lung tissue demonstrating SIV mRNA in cells (red); macrophages, as marked by both CD68 and CD163, (blue); T cells, as marked by CD3 (green); and differential interference contrast (white). (*A*) Centrally caseating lesions and (*B*) nonnecrotizing granulomas in reactivators versus nonreactivators show the presence of numerous virus-infected cells in reactivators, with additional nuclei staining in the bottom images (white). (*C*) Close-up image of white box from *B*. (*D*) Quantification of number of infected cells per field of image in reactivators (R) and nonreactivators (NR). ***$P < 0.001$ using Student's *t* test. (Scale bars, *A*, 250 μ; *B*, 100 μ; and *C*, 25 μ.)

When comparing different subgroups of the relatively few $CD4^+$ T cells in BAL, there was no significant difference in the percentage of central memory ($CD28^+CD95^+$) cells (Fig. 6*D*) or their rate of proliferation, as marked by $Ki67^+$ (Fig. 6*E*). When comparing effector memory cells ($CD28^-CD95^+$), reactivators had a significantly higher percentage of cells in BAL (Fig. 6*F*), albeit the rate of turnover was not significantly different (Fig. 6*G*). As expected, the absolute number of central (T_{CM}) and effector (T_{EM}) memory cells sharply declined after SIV infection, such that both reactivators and nonreactivators retained ∼4% and 5% T_{CM}, and 15% and 13% T_{EM}, respectively (Fig. S3).

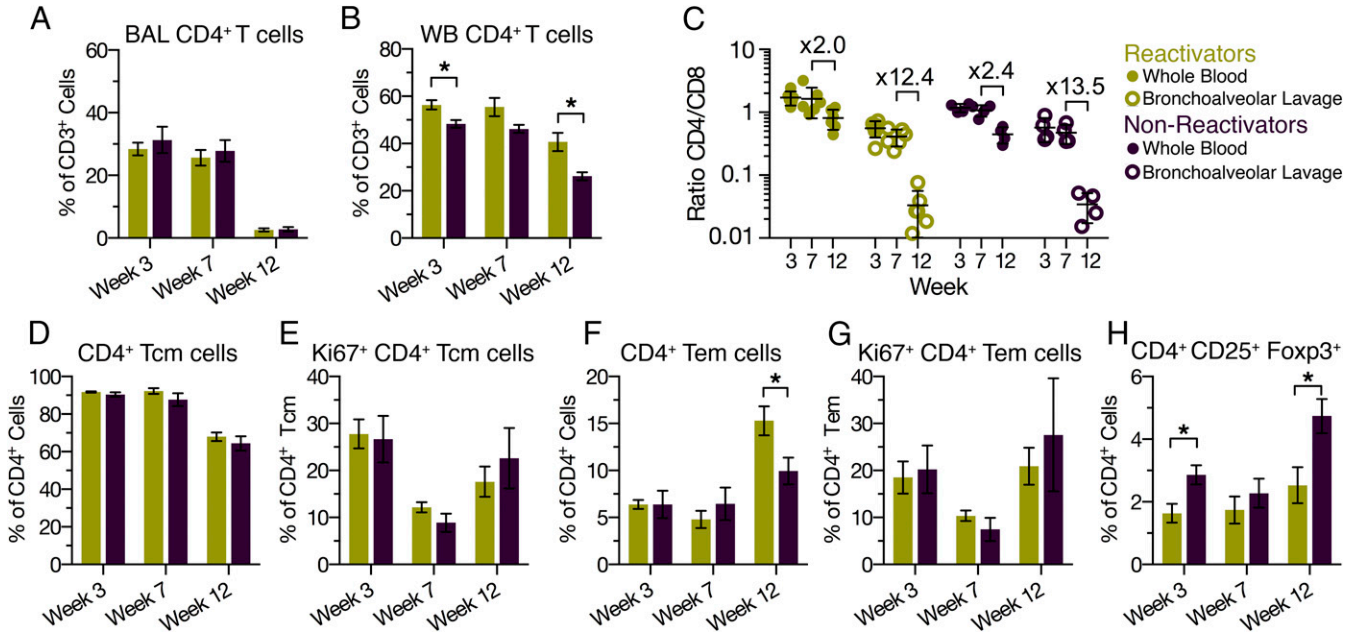

Fig. 6. Comparative $CD4^+$ T-cell responses in reactivators and nonreactivators. Comparison of BAL cells from reactivators and nonreactivators in weeks 3 and 7 after *Mtb* infection and week 3 after SIV infection. Quantification of $CD4^+$ T cells in (*A*) BAL and (*B*) whole blood (WB), as a percentage of all $CD3^+$ T cells. (*C*) Ratio of $CD4^+$:$CD8^+$ T cells in whole blood (closed circles) and in BAL (open circles) with indicated fold-change between week 7 after *Mtb* infection and week 3 after SIV infection. (*D*) Analysis of central memory ($CD28^+CD95^+$) $CD4^+$ T cells and (*E*) their proliferation. (*F*) Analysis of effector memory ($CD28^-CD95^+$) $CD4^+$ T cells and (*G*) their proliferation. (*H*) Percentage of T_{reg} cells responding as a percentage of $CD4^+$ T cells. $^*P < 0.05$ using two-way ANOVA. Data are means ± SD.

When comparing the absolute numbers of memory cells responding, the difference in T_{CM} was not significant between the two groups (Fig. S3), whereas reactivators had significantly more T_{EM} in BAL 7 wk after *Mtb* infection and 3 wk after SIV infection (Fig. S3). Comparison of the number of naive ($CD28^+CD95^-$) cells revealed that reactivators and nonreactivators retained ∼52% and 65%, respectively, indicating that truly naive cells are spared from SIV-induced depletion (Fig. S3). Furthermore, the percentage of $CD4^+$ T regulatory (T_{reg}) cells ($CD25^+Foxp3^+$) found in BAL 3 wk after SIV infection was significantly higher in nonreactivators (Fig. 6*H*). This increase in $CD4^+$ T_{regs} in nonreactivators, coincident with decreased $CD4^+$ T_{EM}, suggests a role for these regulatory cells in limiting disease-causing pathology, which was increased in reactivators (Figs. 3 and 4). Although there were significantly more T_{CM} in the periphery of nonreactivators (Fig. S4), this finding was not observed at the site of infection (Fig. 6*D*). Additionally, there was no marked difference in the percentage of $CD4^+$ T cells in peripheral blood expressing the lymph node homing marker CCR7 or the tissue homing marker CCR5 (Fig. S4).

The percentage of $CD8^+$ T cells recruited to BAL expectedly increased because of SIV coinfection, thus contributing to a sharp decrease in the CD4:CD8 ratio in all coinfected animals, irrespective of their reactivation status (Figs. 6*C* and 7 *A* and *B*). Whereas there was no statistically significant difference in the percentage or the number of central and effector memory $CD8^+$ T cells present in the BAL after coinfection (Fig. 7 *C* and *E*), nonreactivators however had a significantly higher rate of turnover, as marked by *Ki*67$^+$, indicating these cells were active and proliferating (Fig. 7 *D* and *F*). To further study the role of $CD8^+$ T cells at the site of infection, we assessed the extent of granzyme B production by immunohistochemistry. Reactivators displayed significantly reduced production of granzyme B in the lungs compared with the nonreactivators (Fig. 7 *G–I*), indicating a correlation between increased granzyme B production, which occurs at least partly within $CD8^+$ T cells (31, 32), and increased control of both SIV- and TB-associated pathology. Although the majority of cells expressing granzyme B were $CD3^+$ lymphocytes (Fig. 7*H*), natural killer (NK) cells likely represent the $CD3^-$ cells producing granzyme B. We used flow cytometry to further assess whether the disparate responses in the two subgroups following SIV coinfection could result from changes in the profiles of NK T cells (NKT) or NK cells. Changes in the percentage and absolute numbers of NKT ($CD3^+CD8^+CD56^+$) and NK ($CD3^-CD8^+CD56^+$) cells, including subsets expressing perforin, were not significantly different based on the reactivation phenotype (Fig. S5). However, there was a general trend toward slightly greater accumulation of both NKT and NK cells in the lungs of nonreactivators relative to reactivators. Together, these data showing increased proliferation in both the central and effector memory populations lend credence to the roles of $CD8^+$ T cells and granzyme B in the control of *Mtb* infection.

BALT Proximal to Granulomas. We have previously demonstrated that the presence of inducible lymphoid follicles, also termed inducible BALT (iBALT), correlates with protection from TB (33). Animals with LTBI harbor greater areas of iBALT within lung lesions relative to animals with ATB, in which BALT was replaced by neutrophils (34). In our current study, nonreactivators often formed multiple, well-organized areas of lymphoid follicles, as observed by H&E staining, as well as by chromogenic staining against CD20 (Fig. 8 *A–D*). Although there is complete ablation of $CD4^+$ T cells in the lungs, BALT still persisted in nonreactivators, occupying a greater average percentage area of the lungs than in reactivators (Fig. 8 *E* and *F*). Protection strongly correlates with extensive BALT formation as we have observed that macaques mucosally vaccinated with a BALT-inducing isogenic mutant, *Mtb* Δ*sigH*, exhibited complete protection upon lethal challenge (14). Notably, iBALT in nonreactivators exclusively harbored tingible body macrophages (Fig. 8*G*), specialized macrophages that are involved in germinal-center reactions (35) and that are especially critical for the phagocytosis of apoptotic B cells undergoing affinity maturation (36). Overall, our findings indicate that protection from reactivation of *Mtb* infection occurs independently of

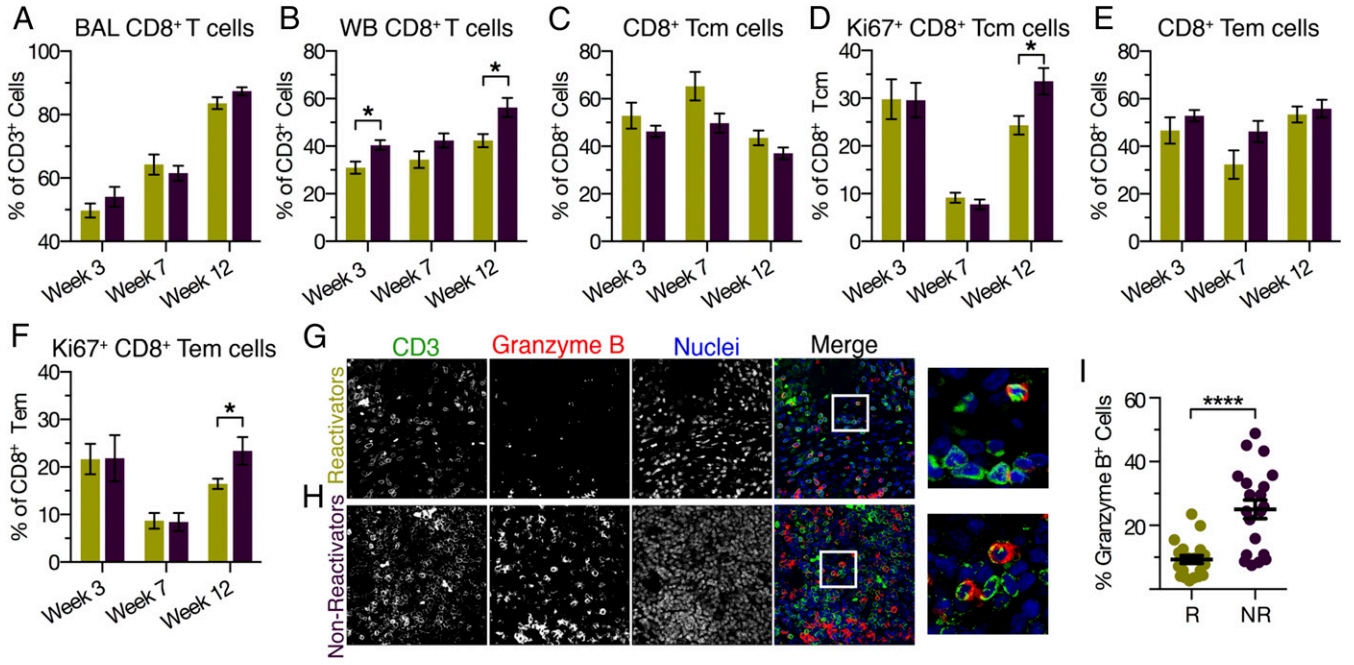

Fig. 7. Proliferative and functional CD8$^+$ T-cell responses. Analysis of CD8$^+$ T cells in (*A*) BAL and (*B*) whole blood, as a percentage of all CD3$^+$ T cells. (*C*) Analysis of central memory CD8$^+$ T cells and (*D*) their proliferation. (*E*) Analysis of effector memory CD8$^+$ T cells and (*F*) their proliferation. Immunohistochemical staining for (*G*) reactivators and (*H*) nonreactivators; in greyscale for (*Left*) CD3, (*Center Left*) granzyme B, and (*Center Right*) nuclei, and in color for (*Right*) merged images of lung sections. Far *Right* panel is a magnified image of the boxed region from the proximal panels. (Magnification, *G* and *H*, 40×.) (*I*) Quantification of the percentage of cells producing granzyme B. *$P < 0.05$; ****$P < 0.0001$ (*A–F*) using two-way ANOVA or (*I*) using Student's *t* test. Data are means ± SD (*A–F, I*) reactivators (R), gold; nonreactivators (NR), purple.

CD4$^+$ T-cell depletion and correlates rather with increased levels of iBALT.

Discussion

One-third of the world's population has LTBI, and yet the mechanisms by which LTBIs are controlled have not been defined. The emergence of the HIV epidemic revealed the significance of CD4$^+$ T cells in controlling TB in humans (1). However, in our study, a subset of coinfected macaques retained control of LTBI despite complete ablation of pulmonary CD4$^+$ T cells. Protection from reactivation correlated with enhanced CD8$^+$ T-cell function, increased iBALT persistence, and the resulting effects on local pathology. The precise roles of these CD4-independent components in HIV coinfected humans warrant further investigations.

Despite contrasting clinical outcomes, every coinfected macaque in our study exhibited indistinguishable pulmonary CD4$^+$ T-cell depletion. Nonreactivating animals had an enhanced effector CD8$^+$ T-cell population, conceivably leading to suppression of both viral replication and SIV-related pathology. In comparison, animals with reactivation TB had lower effector CD8$^+$ T-cell counts and showed increased SIV- as well as TB-associated pathology. To counter immune control, it is highly likely that the two pathogens synergize within the lungs of reactivated animals and exacerbate pathology. This hypothesis is supported by data that reactivators had significantly more SIV-infected cells within the granuloma. In addition, the perivascular lesions were significantly aggravated, had high bacterial burdens, and possibly led to increased bacterial dissemination. Although the colocalization of the virions and the bacilli within the same cells in granulomatous lesions has been described previously (22), their interactions in this local environment remain undercharacterized. We propose that, in reactivators, microenvironmental changes provide specific niches conducive to replication of both pathogens. Based on our findings, we hypothesize that CD8$^+$ T-cell–mediated responses can suppress SIV replication in tuberculous granulomas and limit SIV-induced pathology.

In nonreactivators, both CD8$^+$ T-cell proliferation and function were found to be increased. Whereas the percentages of CD8$^+$ T cells recruited to the lung were similar, the proliferation of central and effector memory CD8$^+$ T cells was significantly enhanced in nonreactivators. Furthermore, granzyme B expression in CD3$^+$ T cells suggests a correlation between the presence of functional CD8$^+$ T cells and protection from SIV-mediated reactivation in primates (32). These results are consistent with previous observations that macaques not only lose bacillus Calmette–Guérin vaccination-induced protective immunity upon experimental depletion of CD8$^+$ T cells, but also reactivate *Mtb* infections suppressed by chemotherapy at a higher rate (13). In addition, the presence of CD3$^-$ cells producing granzyme lends credibility to the role of NK cells in mediating control of both SIV and *Mtb* infection (37, 38). The effector role of CD8$^+$ T cells in the control of *Mtb* infection in humans has recently been described to inversely correlate with bacterial load in sputum (39), and HIV coinfection can impair *Mtb*-specific CD8$^+$ T degranulation and proliferation (40). Thus, the effector roles of CD8$^+$ T cells in curtailing reactivation need to be further investigated.

In addition to CD8$^+$ T cells and altered pathology, we also found that the presence of BALT proximal to the granuloma strongly correlates with control of TB reactivation. Previously, we have shown that increased BALT presence was associated with increased protection in mice, NHPs, and humans (33, 34). More importantly, protective immunity to TB, induced by a novel vaccine, also correlated strongly with the presence of BALT (14). In this study, we showed that the persistence of BALT increased protection from reactivation. Although the precise role of B cells in TB infection control remains to be determined, existing evidence suggests that B cells are required for optimal development of immune responses against *Mtb* (15, 16, 41). Moreover, the presence of tingible body macrophages in BALT suggests that B cells are undergoing affinity maturation or that cross-priming of CD8$^+$ T cells occurs within these lymphoid

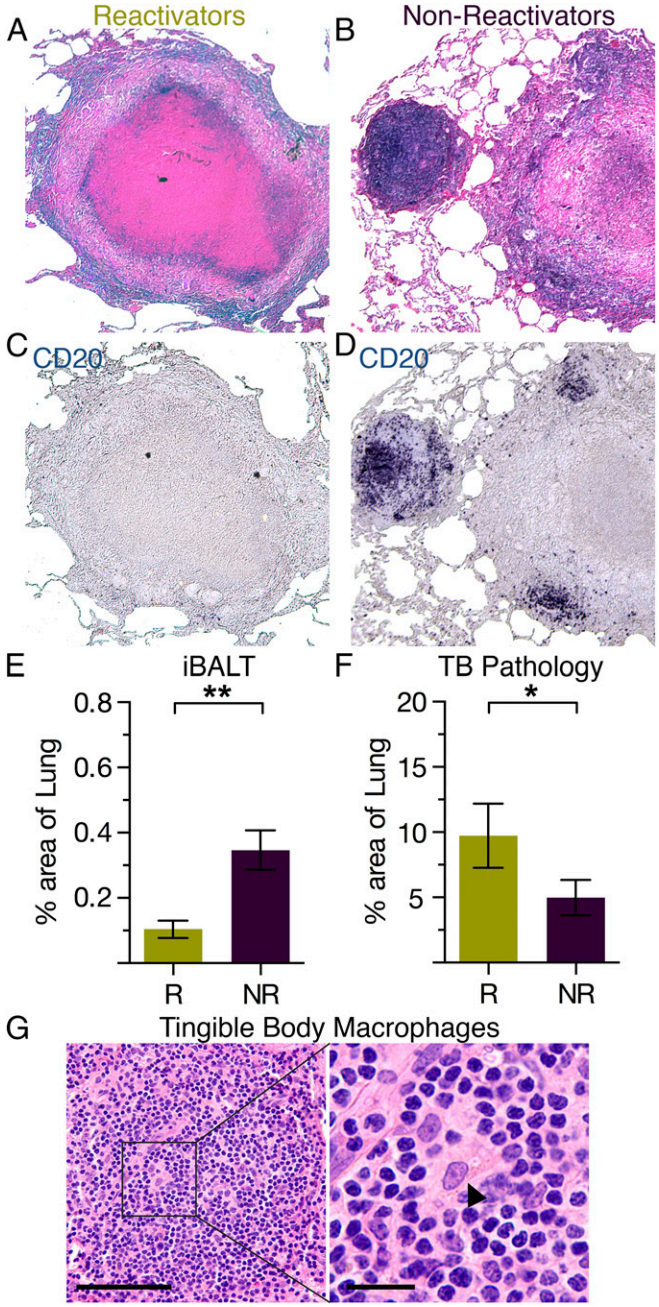

Fig. 8. Persistence of iBALT correlates with protection from reactivation. H&E staining of lung sections from (*A*) reactivating animals and (*B*) nonreactivating animals, with the same sections of lung chromogenically stained in *C* and *D*, respectively, for $CD20^+$ B cells. Quantification of percentage area of (*E*) iBALT formation and (*F*) tuberculosis-associated pathology per lung section in reactivating (R) versus nonreactivating (NR) animals. $*P < 0.05$, $**P < 0.01$, using Student's *t* test. (*G*) H&E staining of tingible body macrophages found in BALT follicles, indicated by the black arrow in the magnified image. [Scale bar, 50 μ (*Left*) and 25 μ (*Right* magnified image).] (Magnification, *A*–*D*, 10×.)

follicles, allowing site-directed activation of macrophages (33, 35, 42, 43). We postulate that these protective lymphoid follicles proximal to the granuloma lead to localized T-cell activation and enhanced B-cell and humoral immunity.

Immune correlates of protective immunity and the mechanism of HIV-induced enhanced susceptibility to reactivation TB are largely unknown. Mechanistic studies into $CD4^+$ T-cell–independent immune control of human TB, particularly the roles of $CD8^+$ T cells, B cells, and the resulting pathologies, are needed. This knowledge will facilitate design of novel interventions against TB, including vaccines and immunotherapeutics.

Materials and Methods

NHP Infection, Sampling, Clinical Procedures, and Euthanasia. All animal procedures were approved by the Institutional Animal Care and Use Committee of Tulane University, New Orleans, LA, and were performed in strict accordance with NIH guidelines. Prior data suggested two different outcomes were possible when latently *Mtb*-infected macaques were exposed to SIV: reactivation in a majority of animals or continued latency in a small subset (22). Thirty-seven specific pathogen-free, retrovirus-free, mycobacteria-naive, adult rhesus macaques that were bred and housed at the Tulane National Primate Research Center (TNPRC) and that ranged from 3 to 12 y of age were assigned to two groups, based on power calculations to detect, with sufficient power, statistically significant differences between the reactivating and nonreactivating groups following coinfection with SIV. All macaques were aerosol-exposed, as described previously (14, 22, 26, 44), to a low dose (~25 CFU implanted) of *Mtb* CDC1551. A subset of the macaques was also exposed approximately 9 wk later to 300 TCID50 (50% tissue culture infectious dose) of SIVmac239 administered intravenously in 1 mL saline, as described previously (22). The control subset received an equal volume of saline intravenously.

Criteria for killing included presentation of four or more of the following conditions: (*i*) body temperatures consistently greater than 2 °F above preinfection values for 3 or more weeks in a row; (*ii*) 15% or more loss in body weight; (*iii*) serum CRP values higher than 10 mg/mL for 3 or more consecutive weeks, CRP being a marker for systemic inflammation that exhibits a high degree of correlation with active TB in macaques (22, 23); (*iv*) CXR values higher than 2 on a scale of 0–4; (*v*) respiratory discomfort leading to vocalization; (*vi*) significant or complete loss of appetite; and (*vii*) detectable bacilli in BAL samples.

Samples were collected before and after *Mtb* infection, as well as after SIV infection. TSTs were performed 1 or 2 wk before infection and at 3 wk after *Mtb* infection, as previously described (22, 23). CXRs were acquired 2 wk before *Mtb* infection and at 3, 7, 11, and 14 wk after *Mtb* infection, as previously described (14, 22). The CXRs were scored by veterinary clinicians in a blinded fashion on a subjective scale of 0–4, with a score of 0 denoting normal lung and a score of 4 denoting severe tuberculous pneumonia, as previously described (14). Before vaccination/infection, all 37 animals received a normal score of 0. Blood was drawn 1 or 2 wk before *Mtb* infection and then weekly thereafter for measuring complete blood count and serum chemistry (22, 26). Blood collected in EDTA tubes (Sarstedt AG & Co.) was used for whole-blood flow cytometry using the panels described earlier (14, 26, 31). BAL samples were obtained, as previously described, 2 wk before *Mtb* infection, again at 3, 7, 11, and 14 wk (22, 26), and then analyzed for CFUs and flow cytometry.

Humane endpoints were predefined in the animal use protocol and applied as a measure of reduction of discomfort (14). The TNPRC Institutional Animal Care and Use Committee approved all animal-related procedures and activities. At necropsy, lung, spleen, and liver tissues were collected and processed, as previously described, using two sections of pulmonary tissue that represented every lung lobe in at least one sample (14); CFU were determined per gram of tissue (22, 26). Lung pathology at necropsy was determined as described previously (22, 26). TB pathology was determined for multiple sections in each lung and averaged for each animal in the study. SIV-induced pathology was reported per section from three reactivators and three nonreactivators, with multiple sections analyzed per animal.

Flow Cytometry. Flow cytometry was performed on whole blood and BAL samples from all animals, as previously described (14, 26, 31).

Immunohistochemistry. Fluorescent immunohistochemistry, chromogenic staining, and in situ hybridization were performed on formalin-fixed, paraffin-embedded tissue, as previously described (45).

Statistical Analyses. Statistical comparisons were performed using one-way or two-way ANOVA in GraphPad Prism with Sidak's correction for multiple hypotheses, or Student's *t* test, as noted in the figure legends and as described previously (14).

ACKNOWLEDGMENTS. This research was supported by NIH awards AI089323, HL106790, and RR026006 (to D.K.), P30110760 (to S.M.), AI111914 (to S.A.K. and D.K.), AI26170 and AI063537 (to W.R.J.), AI094745 (to J.C.), and OD011104 and AI058609 (to the Tulane National Primate Research Center, and a bridge fund by the Tulane Vice President for Research and awards by the Wetmore TB and Leprosy Foundation and the Louisiana Board of Regents).

1. Kwan CK, Ernst JD (2011) HIV and tuberculosis: A deadly human syndemic. *Clin Microbiol Rev* 24(2):351–376.
2. Orme IM, Collins FM (1983) Protection against *Mycobacterium tuberculosis* infection by adoptive immunotherapy. Requirement for T cell-deficient recipients. *J Exp Med* 158(1):74–83.
3. Selwyn PA, et al. (1989) A prospective study of the risk of tuberculosis among intravenous drug users with human immunodeficiency virus infection. *N Engl J Med* 320(9): 545–550.
4. Barnes PF, Bloch AB, Davidson PT, Snider DE, Jr (1991) Tuberculosis in patients with human immunodeficiency virus infection. *N Engl J Med* 324(23):1644–1650.
5. Urdahl KB, Shafiani S, Ernst JD (2011) Initiation and regulation of T-cell responses in tuberculosis. *Mucosal Immunol* 4(3):288–293.
6. Flynn JL, Chan J (2001) Immunology of tuberculosis. *Annu Rev Immunol* 19:93–129.
7. Lenaerts A, Barry CE, 3rd, Dartois V (2015) Heterogeneity in tuberculosis pathology, microenvironments and therapeutic responses. *Immunol Rev* 264(1):288–307.
8. Mehra S, et al. (2013) Granuloma correlates of protection against tuberculosis and mechanisms of immune modulation by *Mycobacterium tuberculosis*. *J Infect Dis* 207(7):1115–1127.
9. Dutta NK, McLachlan J, Mehra S, Kaushal D (2014) Humoral and lung immune responses to *Mycobacterium tuberculosis* infection in a primate model of protection (.). *Trials Vaccinol* 3:47–51.
10. Sia JK, Georgieva M, Rengarajan J (2015) Innate immune defenses in human tuberculosis: An overview of the interactions between *Mycobacterium tuberculosis* and innate immune cells. *J Immunol Res* 2015:747543.
11. Orme IM, Robinson RT, Cooper AM (2015) The balance between protective and pathogenic immune responses in the TB-infected lung. *Nat Immunol* 16(1):57–63.
12. Kamath A, Woodworth JS, Behar SM (2006) Antigen-specific CD8+ T cells and the development of central memory during *Mycobacterium tuberculosis* infection. *J Immunol* 177(9):6361–6369.
13. Chen CY, et al. (2009) A critical role for CD8 T cells in a nonhuman primate model of tuberculosis. *PLoS Pathog* 5(4):e1000392.
14. Kaushal D, et al. (2015) Mucosal vaccination with attenuated *Mycobacterium tuberculosis* induces strong central memory responses and protects against tuberculosis. *Nat Commun* 6:8533.
15. Chan J, et al. (2014) The role of B cells and humoral immunity in *Mycobacterium tuberculosis* infection. *Semin Immunol* 26(6):588–600.
16. Kozakiewicz L, et al. (2013) B cells regulate neutrophilia during *Mycobacterium tuberculosis* infection and BCG vaccination by modulating the interleukin-17 response. *PLoS Pathog* 9(7):e1003472.
17. Zhu Q, et al. (2016) Human B cells have an active phagocytic capability and undergo immune activation upon phagocytosis of *Mycobacterium tuberculosis*. *Immunobiology* 221(4):558–567.
18. Moir S, Chun TW, Fauci AS (2011) Pathogenic mechanisms of HIV disease. *Annu Rev Pathol* 6:223–248.
19. Kanwar B, Favre D, McCune JM (2010) Th17 and regulatory T cells: Implications for AIDS pathogenesis. *Curr Opin HIV AIDS* 5(2):151–157.
20. Hu Z, et al. (2015) HIV-associated memory B cell perturbations. *Vaccine* 33(22): 2524–2529.
21. Patel NR, et al. (2007) HIV impairs TNF-alpha mediated macrophage apoptotic response to *Mycobacterium tuberculosis*. *J Immunol* 179(10):6973–6980.
22. Mehra S, et al. (2011) Reactivation of latent tuberculosis in rhesus macaques by coinfection with simian immunodeficiency virus. *J Med Primatol* 40(4):233–243.
23. Kaushal D, Mehra S, Didier PJ, Lackner AA (2012) The non-human primate model of tuberculosis. *J Med Primatol* 41(3):191–201.
24. Flynn JL, Gideon HP, Mattila JT, Lin PL (2015) Immunology studies in non-human primate models of tuberculosis. *Immunol Rev* 264(1):60–73.
25. Diedrich CR, et al. (2010) Reactivation of latent tuberculosis in cynomolgus macaques infected with SIV is associated with early peripheral T cell depletion and not virus load. *PLoS One* 5(3):e9611.
26. Mehra S, et al. (2015) The DosR regulon modulates adaptive immunity and is essential for *Mycobacterium tuberculosis* persistence. *Am J Respir Crit Care Med* 191(10): 1185–1196.
27. Sharma SK, Mohan A, Sharma A, Mitra DK (2005) Miliary tuberculosis: New insights into an old disease. *Lancet Infect Dis* 5(7):415–430.
28. Aaron L, et al. (2004) Tuberculosis in HIV-infected patients: A comprehensive review. *Clin Microbiol Infect* 10(5):388–398.
29. Li Y, et al. (2015) SIV infection of lung macrophages. *PLoS One* 10(5):e0125500.
30. Mattapallil JJ, et al. (2005) Massive infection and loss of memory CD4+ T cells in multiple tissues during acute SIV infection. *Nature* 434(7037):1093–1097.
31. Phillips BL, et al. (2015) LAG3 expression in active *Mycobacterium tuberculosis* infections. *Am J Pathol* 185(3):820–833.
32. Mazzaccaro RJ, et al. (1998) Cytotoxic T lymphocytes in resistance to tuberculosis. *Adv Exp Med Biol* 452:85–101.
33. Slight SR, et al. (2013) $CXCR5^+$ T helper cells mediate protective immunity against tuberculosis. *J Clin Invest* 123(2):712–726.
34. Gopal R, et al. (2013) S100A8/A9 proteins mediate neutrophilic inflammation and lung pathology during tuberculosis. *Am J Respir Crit Care Med* 188(9):1137–1146.
35. Smith JP, Burton GF, Tew JG, Szakal AK (1998) Tingible body macrophages in regulation of germinal center reactions. *Dev Immunol* 6(3-4):285–294.
36. Kranich J, et al. (2008) Follicular dendritic cells control engulfment of apoptotic bodies by secreting Mfge8. *J Exp Med* 205(6):1293–1302.
37. Shang L, et al. (2014) NK cell responses to simian immunodeficiency virus vaginal exposure in naive and vaccinated rhesus macaques. *J Immunol* 193(1):277–284.
38. Portevin D, Via LE, Eum S, Young D (2012) Natural killer cells are recruited during pulmonary tuberculosis and their ex vivo responses to mycobacteria vary between healthy human donors in association with KIR haplotype. *Cell Microbiol* 14(11): 1734–1744.
39. Silva BD, Trentini MM, da Costa AC, Kipnis A, Junqueira-Kipnis AP (2014) Different phenotypes of CD8+ T cells associated with bacterial load in active tuberculosis. *Immunol Lett* 160(1):23–32.
40. Kalokhe AS, et al. (2015) Impaired degranulation and proliferative capacity of *Mycobacterium tuberculosis*-specific CD8+ T cells in HIV-infected individuals with latent tuberculosis. *J Infect Dis* 211(4):635–640.
41. Achkar JM, Chan J, Casadevall A (2015) B cells and antibodies in the defense against *Mycobacterium tuberculosis* infection. *Immunol Rev* 264(1):167–181.
42. Hey YY, O'Neill HC (2012) Murine spleen contains a diversity of myeloid and dendritic cells distinct in antigen presenting function. *J Cell Mol Med* 16(11):2611–2619.
43. Schaible UE, et al. (2003) Apoptosis facilitates antigen presentation to T lymphocytes through MHC-I and CD1 in tuberculosis. *Nat Med* 9(8):1039–1046.
44. Mehra S, et al. (2010) Transcriptional reprogramming in nonhuman primate (rhesus macaque) tuberculosis granulomas. *PLoS One* 5(8):e12266.
45. Li Q, Skinner PJ, Duan L, Haase AT (2009) A technique to simultaneously visualize virus-specific CD8+ T cells and virus-infected cells in situ. *J Vis Exp* 30(30):e1561.